Electron Energy Loss and DFT/SCI Study of the Singlet and Triplet Excited States and Electron Attachment Energies of Tetramethylsilane, Hexamethyldisilane, Tris(trimethylsilyl)silane, and Tetramethoxysilane

Vroni Huber, Knut R. Asmis, Anne-Christelle Sergenton, and Michael Allan*,†

Institut de Chimie Physique, Université de Fribourg, Pérolles, CH-1700 Fribourg, Switzerland

Stefan Grimme*,‡

Intitut für Physikalische und Theoretische Chemie der Universität Bonn, Wegelerstrasse 12, D-53115 Bonn, Germany

Received: December 16, 1997; In Final Form: February 13, 1998

Singlet and triplet excited states of the title compounds were investigated experimentally, using electron-energy-loss spectroscopy (EELS), and theoretically, using density functional calculations that include configuration interaction (DFT/SCI). Both the triplet and the singlet spectra are well rationalized by the theory, permitting an assignment of the observed, broad bands and providing strong indication that DFT/SCI is suitable for the description of excited states in molecules containing third-row elements. The low-lying transitions in tetramethylsilane are found to be 4s and 4p Rydberg; the lowest valence states are higher, at 9.8 eV (triplet) and 10.5 eV (singlet). The lowest triplet band in hexamethyldisilane is found to be valence, the upper orbital having π symmetry. The lowest singlet state is 4s, albeit with zero oscillator strength. The lowest observed singlet band is $4p_{xy}$ Rydberg with substantial π^* valence admixture. The calculated density of excited states is high in tris(trimethylsilyl)silane, and Rydberg−valence mixing is prevalent. A high density of states is found also for tetramethoxysilane, the low-lying transitions being all Rydberg originating from the oxygen lone pair orbitals. Excitation functions for selected vibrational and electronically excited states are presented. The former provide the electron attachment energies. The latter indicate large cross sections for triplet excitation near threshold and, thus, imply substantial yield of triplet states under typical plasma conditions. The He I photoelectron spectrum of tetramethoxysilane is also presented.

1. Introduction

The present work is concerned with electron-impact excitation, theoretical description of excited states, and electron attachment in four representative alkyl- and alkoxy-substituted silanes (see Chart 1). Interest in the excited states of, and in electron collisions with, this class of compounds is motivated by their industrial use, for example as a silicon carbide or oxide precursors in plasma-assisted chemical vapor deposition.[1] Knowledge of the electronic structure of the simple permethylsilane oligomers is further useful for understanding the higher molecular weight polysilanes, whose chemistry and spectroscopy are of considerable interest.[2]

Photoabsorption spectra of permethylsilanes have been reported both in the gas phase and in solution, and an excellent summary and discussion were given by Robin.[3,4] The photoabsorption spectrum of gas-phase TMOS has also been published.[5] The photoabsorption spectrum of HMDS (and of higher oligomers) in an argon matrix have been recorded by Plitt et al.[6] The valence shell electron-energy-loss (EEL) spectrum of TMS has been recorded at a high incident electron energy (2.5 keV) and in forward scattering by Sodhi et al.[7]

The occupied orbitals of a number of methylsilanes including TMS and HMDS have been characterized by means of photoelectron spectroscopy, reviewed by Bock.[8] The electron attachment energies, characteristic of the orbitals which are not occupied in the neutral molecule, have recently been measured using electron transmission spectroscopy (ETS).[9] The core excitation EEL spectra of TMS, also representative of normally unoccupied orbitals, albeit with a positively charged core, were published by Sodhi et al.[7] and Winkler et al.[10] Urquhart et al.[11] measured core excitation EEL and photoabsorption spectra of TMS, HMDS, and TTMSS.

CHART 1

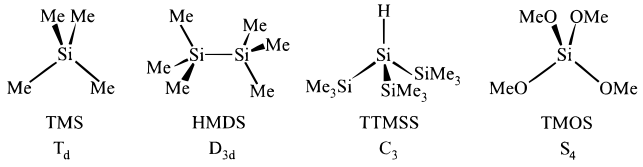

In the present work we apply electron-energy-loss spectroscopy at low incident electron energies, and both forward and backward scattering, to determine the triplet and the singlet transition energies of the title compounds. The observed transitions are assigned by comparison with transition energies and oscillator strengths calculated by the DFT/SCI method. We further derive electron attachment energies from relative cross sections for vibrational excitation. Finally, relative cross sections for electronic excitation are presented as a function of the incident electron energy, permitting conclusions about the relative yields of triplet and singlet states in plasmas.

† E-mail: Michael.Allan@unifr.ch.
‡ E-mail: grimme@rs3.thch.uni-bonn.de.

S1089-5639(98)00537-4 CCC: $15.00
Published on Web 04/28/1998

TABLE 1: Interatomic Distances *R* (Å) and Angles α (deg) Calculated at the HF−SCF Level of Theory by Employing the Basis Sets Described in Section 2.2

	R_{Si-Si}	R_{Si-C}	R_{C-H}	R_{Si-H}	$\alpha_{C-Si-Si}$	α_{C-Si-C}	$\alpha_{Si-Si-Si}$	$\alpha_{H-Si-Si}$
TMS		1.889	1.097					
HMDS	2.381	1.898	1.097		110.5	108.5		
TTMSS	2.389	1.895[a]	1.097[a]	1.504	110.5	108.3	112.8	105.9

	R_{Si-O}	R_{O-C}	R_{C-H}[a]	α_{C-O-Si}	α_{O-Si-O}
TMOS	1.620	1.422	1.091	135.9	107.5

[a] Average values.

2. Methods

2.1. Experimental Section. The trochoidal electron spectrometer used in the present work has been described in detail previously.[12,13] It uses magnetic collimation of the electron beams, trochoidal monochromators as electron energy filters, and a collision chamber with small apertures for the incident and scattered electron beams. The experiment involves intercepting the sample vapor at low pressure ($\sim 10^{-4}$ mbar) with a beam of electrons of varying incident energy E_i and detecting electrons scattered at a fixed residual energy E_r. The incident electrons can excite the target molecules, thereby loosing an amount of kinetic energy $\Delta E = E_i - E_r$ equal to the excitation energy. A spectrum of excited states is obtained by plotting the scattered electron current I_s against the electron energy loss ΔE. The collision chamber was kept at about 60 °C during the measurement, the resolution was about 0.045 eV, and the energy scale is accurate to within 0.03 eV.

This instrument detects electrons scattered into 0° and into 180°.[12,14] Forward scattering generally dominates at higher electron energies, and we can therefore safely assume that at $E_r = 20$ eV the backward scattering cross section is small in relation to the forward cross section, although we have not measured the forward/backward signal ratios in the present case. The observed spectra are thus due nearly exclusively to electrons scattered in the forward direction. Dipole selection rules apply to excitation by electron impact in the limit of forward scattering and high electron energies (nearly zero momentum transfer). The residual energy of 20 eV is sufficiently high to make the spectra recorded at this energy dominated by dipole-allowed transitions and band intensities indicative of the dipole oscillator strengths. The electron energy is not high enough for the dipole limit to be reached quantitatively, the relative intensities of the bands may differ from the dipole intensities, and dipole forbidden singlet transitions may also appear in the spectra (an example is the $a^1\Pi_g$ state of N_2[12]). A qualitative comparison of band intensities with calculated and measured oscillator strengths is, however, meaningful. The qualitative nature of the band intensity comparison with calculated oscillator strengths does not justify conversion of the vertical scale of the spectra to generalized oscillator strength, and we choose to show the unconverted signal intensity, corresponding to a (relative) differential cross section (DCS). When comparing EEL band intensities and oscillator strengths, it is useful to realize that bands at higher energy loss would appear more intense in the generalized oscillator strength representation than they do in the DCS representation.

Triplet bands appear in the spectra recorded with low residual energies. The cross sections for excitation of the triplet states are furthermore not forward peaked, but more isotropic with respect to scattering. The capacity of the present instrument to detect the backward scattered electrons is thus essential for the detection of triplet states.

2.2. Computational Details. The method for describing excited states of closed-shell molecules using density functional calculations combined with a single-excitation configuration interaction treatment (DFT/SCI) has been developed recently.[15] It is superior to the standard ab initio HF/SCI approach due to the implicit account of dynamical electron correlation. The errors in the excitation energies of Rydberg and valence excited states, obtained with this method, were found not to exceed 0.2 eV for a wide range of molecules.[15] Particularly important for the present study is the capacity of this method to treat well valence−Rydberg mixing, as has been demonstrated on ethene, methanal,[16] and substituted ethenes,[17] which are quite difficult to describe with standard ab initio approaches.

All Hartree−Fock (HF−SCF) and DFT calculations were performed with the TURBOMOLE suite of programs.[18,19] The ground-state geometries of the molecules were completely optimized at the HF−SCF level by employing valence double-ζ basis sets for the carbon, oxygen, and hydrogen atoms (VDZ, [3s2p]/[2s])[20] and a triple-ζ basis including polarization d-functions for silicon (TZP, [4s3p1d]).[20] The geometrical parameters obtained are given in Table 1. The calculated SiC bond distance in TMS of 1.889 Å agrees well with the experimental value of 1.879 Å.[21] Due to steric interactions of the methyl groups in TTMSS the structure has only C_3 symmetry (instead of C_{3v}) with deviations of the dihedral angles H−Si−Si−C from C_{3v} symmetry of about 15°.

The DFT calculations were performed with the nonlocal exchange correlation functional of Becke and Lee, Yang, and Parr in its hybrid form, i.e., including some portion of exact HF exchange (B3LYP).[22,23] In the DFT/SCI calculations of the excited states the silicon basis was augmented with one set of primitive s; p-, and d-functions $\alpha_s = 0.015$, $\alpha_p = 0.013$, and $\alpha_d = 0.010$ to account for the lowest Rydberg states. Ground-state geometries were employed throughout all excited-state calculations so that all theoretical excitation energies represent vertical transitions.

The carbon, oxygen, and hydrogen atom VDZ basis sets were replaced by those of Dunning[24] (because the lowest s- and p-exponents are better suited for a description of excited states) and in the case of carbon and oxygen augmented with a polarization d-function. The complete molecular basis sets used to expand the Kohn−Sham equations are thus comprised of 116, 192, 326, and 172 AOs for TMS, HMDS, TTMSS, and TMOS, respectively.

The SCI calculations were performed in the C_{2v}, C_{2h}, C_1, and C_2 subgroups of the full T_d, D_{3d}, C_3, and S_4 point groups, respectively. The 1s, 2s, 2p(Si), and 1s(C) core electrons are kept frozen while all valence and virtual orbitals are used to construct the spin-adapted configuration state functions (1457, 3776, 9321, and 3669 ignoring symmetry for TMS, HMDS, TTMSS, and TMOS, respectively).

All transition moments were calculated in the dipole length form, which is preferable over the dipole velocity form in the case of very approximate wave functions.[25] Formal oscillator

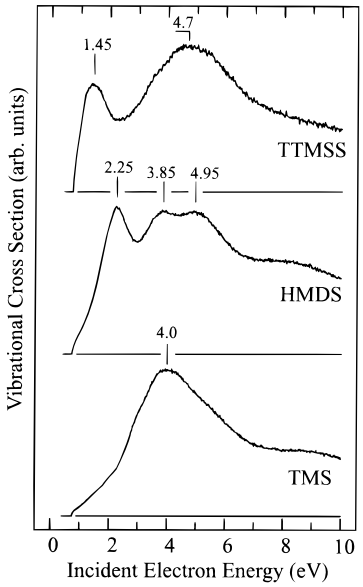

Figure 1. Vibrational excitation functions, recorded at an energy loss of 0.72 eV.

TABLE 2: Experimental Electron Attachment Energies and DFT MO Energies (eV)

compd	present	Modeli et al.[9]	DFT MO energy
TMS	4.0	3.8	3.2 (σ*(Si−C))
HMDS	2.25	2.30	1.7 (π*)
	3.85	4.1	2.8 (σ*(Si−Si))
	4.95		
TTMSS	1.45	1.49[a]	0.7 (Si−Si)
	4.7	2.9[a]	
TMOS	∼2		2.15

[a] $MeSi(SiMe_3)_3$.

strengths (i.e. ignoring electron spin and using only the space part of the triplet wave functions) were calculated also for the triplet states.

3. Results and Discussion

3.1. Electron Attachment Energies. We employed the vibrational excitation functions to measure the attachment energies, making use of the fact that the cross section for vibrational excitation generally dramatically increases when an electron is temporarily attached to the target molecule, i.e., when a shape resonance is encountered in the scattering.[26] The attachment energies of substituted silanes have already been measured using ETS,[9] but the present method, being a "zero background" technique, is sometimes better suitable for detecting broad resonances. The excitation functions are shown in Figure 1. To ascertain that all bands in Figure 1 are indicative of resonances, we recorded the excitation functions at a relatively large energy loss, where only overtone vibrations are excited. This avoids bands at low energy caused by nonresonant excitation of IR-active fundamentals. The energy loss of 0.72 eV corresponds nominally to two quanta of the C−H stretch vibration, but the shape of the energy-loss spectra indicates that additional, overlapping vibrations are also excited.

The attachment energies are summarized and compared with the ETS results of Modeli et al.[9] in Table 2. The agreement of the two data sets is very good—small differences can be expected because the resonances are observed in different final channels in the two experiments. The somewhat higher value found for TMS could indicate that the broad band consists of two or more overlapping resonances, the relative heights of which differ in the two experiments.

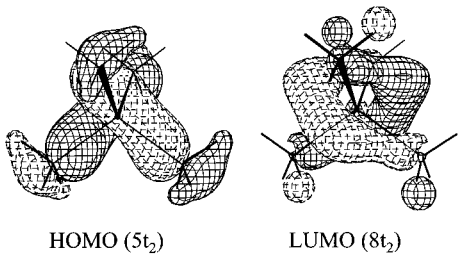

Figure 2. Isocontour plots of the HOMO and the valence LUMO of TMS. The plots refer to an isosurface value of $|\psi| = 0.06$ au. Only one component of the degenerate orbitals is shown.

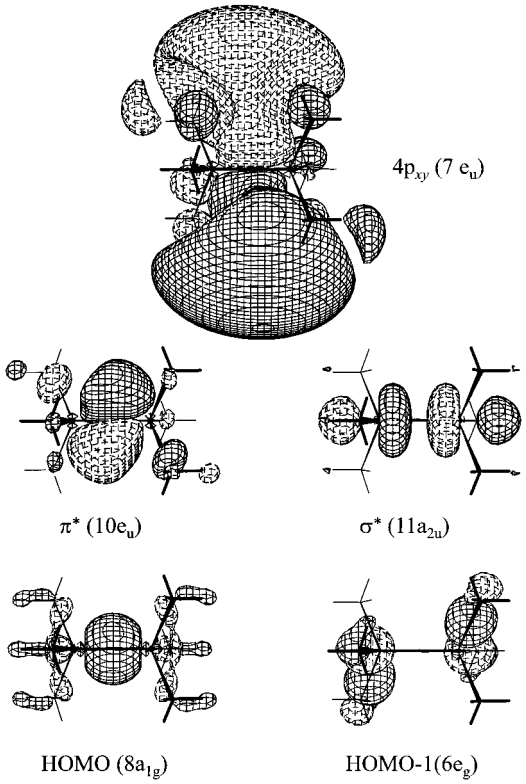

Figure 3. Isocontour plots of selected molecular orbitals of HMDS. The valence (Rydberg) orbital plots refer to an isosurface value of $|\psi| = 0.06$ au (0.01 au). Only one component of the degenerate orbitals is shown. The Rydberg orbital is much larger than the valence orbitals: the $\langle r^2 \rangle$ values for the HOMO-1, HOMO, π*, and $4p_{xy}$ orbitals are 23.4, 16.0, 44.9, and 103.8 a_0^2, respectively.

We notice that the DFT virtual orbital energies qualitatively rationalize the AEs (Table 2) and base our assignment on this comparison. [Our attempts to rationalize the attachment energies with help of SCF virtual orbital energies and an empirical scaling relation (an approach which proved successful with many compounds not containing third-row elements) did not lead to satisfactory results for the silanes.] Schematic diagrams of high-lying occupied and low-lying unoccupied orbitals of TMS and HMDS are shown in Figures 2 and 3. The lowest attachment in HMDS is assigned to a π* orbital. (We add an asterisk to the orbital symbol for consistency with previous literature and to indicate that it is normally unoccupied. This MO is, however, bonding with respect to the Si−Si distance, in contrast to the π* MO of, for example, ethene, which is antibonding with respect to the C=C bond.) This assignment does not contradict the finding made elsewhere that the lowest empty MO in higher alkylsilane oligomers and polymers is σ*(Si−Si).[2] Modeli et

al.[9] note that ab initio 3-21G* virtual orbital energies predicts π^* below σ^* in HMDS, whereas semiempirical MNDO method leads to the reversed order.

It is interesting to note that the assignment π^* below σ^* in HMDS parallels that recently made for cyclopropane, where the observed selectivity of vibrational excitation led to the assignment of the lowest electron attachment (at 2.6 eV) to a similar C−H antibonding but C−C bonding π^* orbital,[33] whereas the attachment to the σ^*(C−C) MO has been unambiguously proven to lie at higher energy (5.5 eV) by the observed angular distribution of the scattered electrons.[34]

The vibrational excitation functions of TMOS (not shown) do not have a well-developed structure; they consist of two strongly overlapping and very broad bands, peaking at about 2 and 6 eV. The former is compatible with the DFT σ^* virtual orbital energy (lowest valence MO) of 2.15 eV.

Core excitation spectra, either energy loss or photoabsorption, provide alternative information on normally unoccupied orbitals, with the difference that the core is positively charged whereas it is neutral in the present electron attachment spectra. As a consequence, Rydberg orbitals appear in the former but are missing in the latter. A broad band observed in the Si(2p) excitation spectrum of TMS has been assigned as overlapping valence and Rydberg states.[7,10] Individual bands can be discerned in photoabsorption spectra of TMS and have been assigned as 4s, 4d, and 5d Rydbergs, followed by σ^*(Si−C) valence orbitals.[11] A lower energy feature emerges in both the core photoabsorption and the core excitation EEL spectra when going from TMS to HMDS, an observation which parallels the low-energy electron attachment band of HMDS in Figure 1. It has been assigned to a valence orbital associated with the Si−Si bond, but it has been labeled σ^*(Si−Si).[11]

3.2. EEL Spectra. A series of spectra with residual energies E_r ranging from 0.03 to 20 eV were recorded for each compound. The best visibility of the triplet states was found with $E_r = 0.1$ eV, and these spectra are shown in Figures 4 and 5, together with the $E_r = 20$ eV spectra, representative for the dipole-allowed singlet transitions.

The lowest singlet band in TMS is broader than the first singlet bands of HMS and TTMSS. Closer inspection reveals a peak at 7.45 eV and a shoulder at 7.2 eV. This shape is presumably a manifestation of the Jahn−Teller splitting of the lowest $1T_2$ state.

The spectra of TMS and HMDS taken at $E_r = 20$ eV agree well with the published gas-phase UV absorption spectra[3,28] both in terms of transition energies and, when it is taken into account that a conversion from DCS to generalized oscillator strength would increase the relative intensity of the higher energy bands, also in terms of relative band intensities. There are only small differences—for example the shoulder at 7.1 eV in HMDS is less pronounced in the UV spectra than in EELS—that could be ascribed to the less stringent selection rules for electron impact excitation at a relatively low incident electron energy.

The $E_r = 20$ eV spectrum of TMOS agrees well with the published gas-phase UV absorption spectrum[5] up to an energy of about 7.8 eV. Both UV and EEL spectra have a weak shoulder with an onset around 6.3 eV, followed by an upward break of slope at about 7 eV. Above 7.8 eV, however, the spectra differ dramatically, and the intense UV bands with sharp vibrational structure are missing in the EEL spectra. We observe that the sharp UV bands are nearly identical in shape and energy to the sharp UV bands of methanol given by the same authors[5]

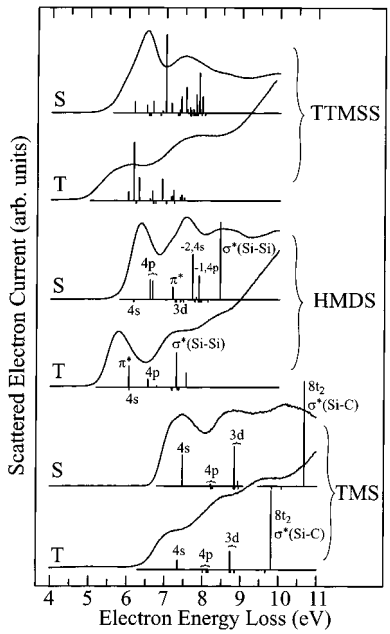

Figure 4. Electron-energy-loss spectra of TMS, HMDS, and TTMSS. Two spectra are shown for each compound, one recorded with $E_r = 20$ eV ("singlet conditions", label S), one with $E_r = 0.1$ eV ("triplet conditions", label T). Vertical lines under the spectra show results of DFT/SCI calculations. Short vertical lines below the baseline indicate transitions with a very small or zero oscillator strength. Selected transitions are labeled. Only the final orbital is given for transitions originating from HOMO, the transition HOMO-2 → 4s and HOMO-1 → 4p are labeled as −2,4s and −1,4p, respectively. (See Tables 3−7 for details of the assignment.)

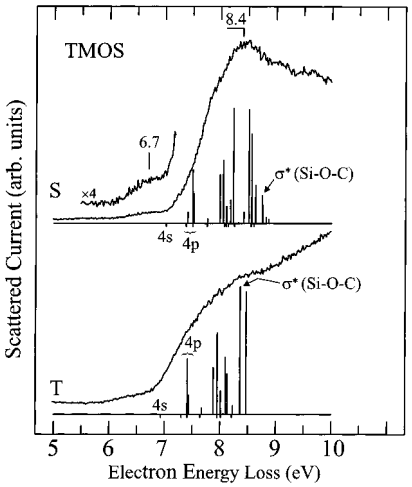

Figure 5. Electron-energy-loss spectrum of TMOS. See the caption of Figure 4.

and that they could consequently be due to methanol impurity resulting from partial hydrolysis of the TMOS sample in the UV cell.

A further verification of this conclusion is provided by a photoelectron spectrum, because the shape and vibrational structure of Rydberg bands is generally nearly identical to that of the ionic state to which they converge. We recorded the He I photoelectron (PE) spectrum (which has, to the best of our knowledge, not been published before) and show it in Figure 6. The purity of the sample was verified using NMR and the index of refraction. No ionic states with sharp vibrational structure are found in the PE spectrum, making the presence of bands with sharp vibrational structure in the UV or EEL spectra highly unlikely.

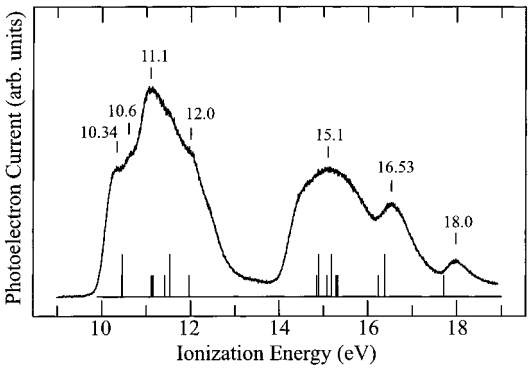

Figure 6. He I photoelectron spectrum of TMOS. Experimental ionization energies are given above the spectrum. Ionization energies calculated within Koopmanns' theorem as DFT orbital energies shifted by 3.3 eV (see section 3.2) are indicated by bars under the spectrum (bars with double height indicate degenerate MOs).

We interpret the PE spectrum within the concept of the Koopmanns' theorem. Although it has been shown for exact solutions of the exchange correlation potential in DFT that Koopmanns' theorem is applicable to the highest occupied molecular orbital,[29] the effect of this result with approximate functionals is not completely clear at present. In particular, all popular functionals suffer from a spurious electron self-interaction[30] causing an incorrect behavior of the potential at large nuclear−electron distances and thus too high energies of the occupied orbitals. Although the admixture of "exact" exchange to the functional (as in B3LYP which is used here) partly corrects this behavior, test calculations on a number of organic molecules show that calculated ionization energies from Kohn−Sham orbital energies are systematically too high by 2−3 eV.[31]

However, as can be seen from a comparison of the experimental PES of TMOS with the calculated DFT orbital energies shifted by 3.3 eV (Figure 6), the relative energies, i.e., the spacing between the four bands, are described very well. The lowest band in the PES between 10 and 13 eV corresponds to ionization out of the oxygen lone-pair orbitals. The MOs that contribute to the next band (14−16 eV) are assigned as π_{O-CH_3}. The two remaining peaks around 16.5 and 18 eV correspond to ionization out of delocalized σ MOs. The weak shoulder at 10.6 eV could be due to Jahn−Teller splitting of the ground state of the ion.

3.3. Comparison with DFT/SCI Results. Excited states have been calculated within the first about 3 eV of each spectrum, and the results are compared with experiment in Tables 3−8 and represented graphically in Figures 4 and 5. Formal oscillator strengths for the triplet states are included in the Figures 4 and 5 and Tables 4 and 6 to point out the interesting empirical finding that they reflect qualitatively the triplet band intensities in the silanes.

A very satisfactory agreement is found for the $E_r = 20$ eV spectrum and the calculated singlet states of TMS. The three strong calculated transitions, from HOMO to 4s, 3d Rydberg (we call the lowest Rydberg states in the silanes 4s, 4p, and 3d to retain consistency with the majority of the literature), and σ^* valence MOs, agree very well with the three broad observed bands at 7.45, 8.8, and 10.15 eV. A similar degree of agreement is found for the triplet spectra. The spectral profiles of HMDS are also well reproduced by the theory, although the calculated energies are generally 0.2−0.3 eV higher than the observed bands. Thus the first singlet band at 6.35 eV corresponds to the two calculated HOMO → 4p transitions, the second band at 7.54 eV to HOMO-2 → 4s and HOMO-1 → 4p transitions, the third band at 8.5 eV to HOMO → σ^*, and the weak shoulder at 7.1 eV fits well the calculated HOMO → π^* transition. The density of states calculated for TTMSS is much higher than for the previous compounds. Despite the large number of states, the calculated transitions are found to be consistent with the spectral envelope, although they appear to be about 0.4 eV higher than observed bands. Thus the onset of the first singlet band is much more gradual in TTMSS than in HMDS. This is consistent with the theoretical result that the intense 5E transition at 7 eV (which corresponds without doubt to the intense peak at 6.5 eV) is preceded by three weaker transitions. The second singlet band, at 7.5 eV, is explained by the cluster of calculated transitions centered around 7.8 eV.

Band overlap is severe in TMOS (Figure 5), but even here the calculation explains well the observed spectral envelope. The weak shoulder at 6.7 eV is assigned as the HOMO → 4s transition, which has calculated oscillator strength of zero but can be expected to be weakly allowed by vibronic interaction with higher states. The signal rise above 7 eV is well explained by the three allowed 4p transitions calculated at 7.41−7.52 eV, and finally the broad peak at 8.4 eV is rationalized by the group of 10 transitions in the 8−8.8 eV range (Figure 5 and Table 8).

TABLE 3: Singlet Transition Energies of TMS[a]

experiment	DFT/SCI				
ΔE_v	ΔE^b	$1000f$	$\Delta\langle r^2\rangle^c$	assignment	
7.45	7.47	209	49	4s	$1T_2$
	8.21	15	82	4p	$2T_2$
	8.22	0	82	4p	$1T_1$
	8.23	0	82	4p	1E
	8.27	0	85	4p	$2A_1$
	8.82	0	150	$3d_{xy,xz,yz}$	$2T_1$
	8.84	0	152	$3d_{xy,xz,yz}$	2E
8.8	8.84	265	153	$3d_{xy,xz,yz}$	$3T_2$
	8.85	0	153	$3d_{xy,xz,yz}$	7A
	8.93	35	159	$3d_{x^2-y^2,z^2}$	$4T_2$
	8.94	0	159	$3d_{x^2-y^2,z^2}$	$3T_1$
	9.82	0	44	HOMO-1 → 4s	$4T_1$
	10.08	0	22	$8t_2$ (valence)	$5T_1$
10.15	10.67	708	40	$8t_2$ (valence)	$5T_2$

[a] Given are the experimental vertical transition energies (ΔE_v, eV, uncertainty ±0.1 eV), the theoretical vertical transition energies ΔE (eV), oscillator strengths f (sum of the oscillator strengths of two components is given for degenerate states), and the difference of ground- and excited state $\Delta\langle r^2\rangle$ expectation values (a_0^2). Only the final MO is indicated for transitions originating from HOMO. [b] The DFT-B3LYP/TZP+diff.(Si)/VDZP(C)/VDZ(H) ground-state energy is −449.0431 au. [c] The $\langle r^2\rangle$ expectation value of the ground state is 94.3 a_0^2.

TABLE 4: Triplet Transition Energies of TMS[a]

experiment	DFT/SCI				
ΔE_v	ΔE	$1000f$	$\Delta\langle r^2\rangle$	assignment	
7.15	7.35	345	48	4s	$1T_2$
	8.01	0	80	4p	$1A_1$
	8.12	19	80	4p	$2T_2$
	8.16	0	82	4p	1E
	8.17	0	82	4p	$1T_1$
8.5	8.73	0	146	$3d_{xy,xz,yz}$	$2T_1$
	8.73	666	147	$3d_{xy,xz,yz}$	$3T_2$
	8.74	0	147	$3d_{xy,xz,yz}$	$2A_1$
	8.75	0	147	$3d_{xy,xz,yz}$	2E
	8.85	26	159	$3d_{x^2-y^2,z^2}$	$4T_2$
	8.86	0	159	$3d_{x^2-y^2,z^2}$	$3T_1$
	9.66	0	43	HOMO-1 → 4s	$4T_1$
9.6	9.81	2880	25	$8t_2$ (valence)	$5T_2$

[a] See the caption of Table 3. Formal oscillator strengths have been calculated by employing only the space part of the triplet wave function.

TABLE 5: Singlet Transition Energies of HMDS[a]

experiment	DFT/SCI				
ΔE_v	ΔE^b	$1000f$	$\Delta\langle r^2\rangle^c$	assignment	
	6.16	0	61	4s	$2A_{1g}$
6.35	6.59	133	64	$4p_{x,y}$	$1E_u$
	6.66	124	95	$4p_z$	$1A_{2u}$
7.1	7.19	83	34	π^*(valence)	$2E_u$
	7.26	0	139	$3d_{xz,xy}$	$1E_g$
	7.28	0	143	$3d_{z^2}$	$3A_{1g}$
	7.39	0	156	$3d_{x^2-y^2,z^2}$	$2E_g$
	7.47	0	58	HOMO-1 → 4s	$3E_g$
7.54	7.71	305	63	HOMO-2 → 4s	$3E_u$
	7.77	0	198	$4f^d$	$2A_{2u}$
	7.78	0	172	5s	$4A_{1g}$
	7.81	14	209	$4f^d$	$4E_u$
	7.86	1	208	$4f^d$	$5E_u$
	7.88	159	68	HOMO-1 → $4p_{x,y}$	$3A_{2u}$
	7.90	0	56	HOMO-1 → $4p_{x,y}$	$1A_{1u}$
	7.94	10	67	HOMO-1 → $4p_{x,y}$	$6E_u$
	8.12	0	244	$4f^d$	$4E_g$
	8.12	2	80	HOMO-1 → $4p_z$	$7E_u$
8.6	8.44	523	39	σ^*(Si−Si)	$4A_{2u}$

[a] See the caption of Table 3. [b] The DFT-B3LYP/TZP+diff.(Si)/VDZP(C)/VDZ(H) ground-state energy is −818.2982 au. [c] The $\langle r^2\rangle$ expectation value of the ground state is 155.9 a_0^2. [d] f-orbitals were built from linear combinations of the Rydberg basis AOs on the two silicon atoms. Not all HOMO → 4f components have been calculated.

TABLE 6: Triplet Transition Energies of HMDS[a]

experiment	DFT/SCI				
ΔE_v	ΔE	$1000f$	$\Delta\langle r^2\rangle$	assignment	
5.78	6.05	765	11	π^*(valence)	$1E_u$
	6.06	0	61	4s	$1A_{1g}$
	6.55	294	92	$4p_z$	$1A_{2u}$
	6.78	40	86	$4p_{x,y}$	$2E_u$
	7.17	0	135	$3d_{xz,yz}$	$1E_g$
	7.19	0	143	$3d_{z^2}$	$2A_{1g}$
7.25	7.30	1250	8	σ^*(Si−Si)	$1A_{2u}$
	7.32	0	155	$3d_{x^2-y^2,z^2}$	$2E_g$
	7.36	0	62	HOMO-1 → 4s	$3E_g$
	7.56	516	58	HOMO-2 → 4s	$3E_u$

[a] See the caption of Table 3. Formal oscillator strengths have been calculated by employing only the space part of the triplet wave function.

TABLE 7: Selected Singlet Transition Energies of TTMSS[a]

experiment	DFT/SCI				
ΔE_v	ΔE^b	$1000f$	$\Delta\langle r^2\rangle^c$	assignment	
∼5.9	6.17	76	70	4s	1E
	6.49	53	50	$4p_z$	2E
	6.66	80	100	$4p_{x,y}$	3E
6.5	6.99	530	109	$3d_{x^2-y^2,z^2}$ (+valence)	5E

[a] 60 roots are calculated below 8 eV, and only transitions below 7 eV and with oscillator strength greater than 0.02 are listed here. See also the caption of Table 3. [b] The DFT-B3LYP/TZP+diff.(Si)/VDZP(C)/VDZ(H) ground-state energy is −1517.5245 au. [c] The $\langle r^2\rangle$ expectation value of the ground state is 263.2 a_0^2.

We conclude that, although the observed bands often correspond to several overlapping transitions, the DFT/SCI calculations rationalize very successfully all spectral profiles, except that the calculated energies become slightly too high as the number of Si−Si bonds increases. Tentatively, this error can be traced back to the inability of current density functionals to treat electron correlation in third and higher row elements. Similar effects have also been observed in DFT calculations of bond lengths becoming much too long if heavier elements are involved (see e.g. ref 27).

TABLE 8: Singlet Transition Energies of TMOS[a]

experiment	DFT/SCI				
ΔE_v	ΔE^b	$1000f$	$\Delta\langle r^2\rangle^c$	assignment	
∼6.7	7.02	0	46	4s	1E
	7.38	0	80	$4p_{x,y}$	2A
	7.41	3	86	$4p_{x,y}$	1B
	7.50	0	83	$4p_{x,y}$	3A
	7.50	15	82	$4p_{x,y}$	2B
	7.52	9	85	$4p_z$	2E
	7.76	0	53	HOMO-1 → 4s	4A
	7.77	1	50	HOMO-2 → 4s	3B
	7.99	14	88	(Rydberg)	3E
	8.05	18	121	$3d_{x^2-y^2}$	4E
	8.06	0	68	HOMO-3 → 4s	5A
	8.08	1	145	$3d_{xz,yz}$	4B
	8.10	0	125	$3d_{xz,yz}$	6A
	8.11	5	138	$3d_{xz,yz}$	5B
	8.13	0	145	$3d_{xz,yz}$	7A
	8.14	0	138	$3d_{xy}$	5E
8.4	8.18	7	148	$3d_{z^2}$	6E
	8.23	33	92	HOMO-2, 3 → $4p_{x,y}$	7E
	8.25	0	96	HOMO-1 → $4p_z$	6B
	8.28	0	89	HOMO-2 → $4p_z$	8A
	8.32	0	81	HOMO-2, 4 → $4p_{x,y}$	8E
	8.42	3	79	HOMO-3, 5 → $4p_z$	7B
	8.51	32	82	HOMO-3 → $4p_{x,y}$	9E
	8.55	0	89	HOMO-4 → $4p_{x,y}$	9A
	8.56	26	88	HOMO-4 → $4p_{x,y}$	8B
	8.60	0	87	HOMO-4 → $4p_{x,y}$	9B
	8.61	0	86	HOMO-4 → $4p_{x,y}$	10A
	8.63	11	86	HOMO-4 → $4p_z$	10E
	8.75	8	51	σ^*(Si−O−C)	11E

[a] See the caption of Table 3. [b] The DFT-B3LYP/TZP+diff.(Si)/VDZP(C)/VDZ(H) ground-state energy is −749.9699 au. [c] The $\langle r^2\rangle$ expectation value of the ground state is 124.8 a_0^2.

The good agreement of the experimental and calculated spectra justifies an assignment based entirely on calculation; it is indicated in Tables 3−8. The singlet state assignment is based on comparison of both the transition energies and the oscillator strengths with the observed spectrum. Since we do not have a theoretical indication of the triplet band intensities, the triplet state assignment is based solely on the comparison of energies. The broad 8.5 eV band in the TMS triplet spectrum, for example, is assigned to the HOMO → 3d transitions, calculated to lie between 8.73 and 8.86 eV (Table 4), but we cannot decide to what degree the individual 3d transitions do contribute to the observed band. We note, however, that the triplet band intensities appear to correlate surprisingly well with the formal oscillator strengths for all four silanes studied here, although we do not attempt to rationalize this observation theoretically at this point.

The resulting assignment implies that all low-lying singlet and triplet excited states of TMS are Rydberg states. The lowest valence states, leading from HOMO to the $8t_2$ (σ^*(Si−C), Figure 2) orbital, are at about 9.5 eV (triplet) and 10.5 eV (singlet). Note that, remarkably, our assignment of the singlet states in TMS confirms in most points the earlier conclusions of Robin,[3] who assigned the first two photoabsorption bands as 4s and 3d and concluded that the 4p transition is hidden under the absorption at around 8 eV, in accordance with the present calculation (Figure 4). He also correctly predicted that the allowed component of the lowest valence transition HOMO → σ^* corresponds to the third band, which peaks at 10.15 eV in the present spectra (and at 10.8 eV in photoabsorption, the difference being an understandable consequence of the large width of the band and the different "background slopes" of electron-impact and photoabsorption cross sections). The

forbidden component of the lowest valence transition is found 0.6 eV below the allowed component by the present calculation (Table 3). The tentative suggestion of Robin that the forbidden component could be seen as a small step at 6.63 eV in the photoabsorption spectrum of Harada[28] (which is not found in our EEL spectrum) is thus not confirmed.

The lowest triplet state of HMDS has valence character, corresponding to excitation from HOMO to the π^* orbital (Figure 3). The medium-sized S−T splitting for this state (1.1 eV) is a consequence of the relative large spatial overlap between the σ and the π^* orbitals (large exchange integral $K_{\sigma-\pi^*}$). The lowest excited singlet state of HMDS is the 4s Rydberg state, but the transition has zero oscillator strength. The first observed singlet band is assigned to two Rydberg states ($4p_{xy}$ and $4p_z$), and the shoulder at 7.1 eV is assigned to the HOMO → π^* valence state. This assignment may initially appear to contradict the conclusion made by Pitt[32] (based on trends in ionization energies), by Robin[3] (based on absence of solvent shift), and by Michl[2] that the first singlet band is of valence character. It should be pointed out, however, that the $4p_{xy}$ states, responsible for the first band according to the present calculation (together with $4p_{xy}$), and the lowest valence state (π^*) both have E_u symmetry and will mix with each other. The degree of mixing is reflected by the spatial extent of the wave functions, expressed by $\Delta\langle r^2\rangle$ (difference of excited-state and ground-state $\langle r^2\rangle$ expectation values). In general Rydberg states of small- and medium sized molecules have $\Delta\langle r^2\rangle$ values in the range 40−60, 80−100, and 100−150 a_0^2 for s, p, and d terms, respectively. This rule is confirmed in the present case: $\Delta\langle r^2\rangle$ is 11 a_0^2 for the pure valence state ^3E_u (Table 6) and 95 a_0^2 for the pure Rydberg state $4p_z$ (Table 5). The intermediate values of 64 and 34 a_0^2 calculated for the ^1E_u and $^1{}^2E_u$ states, respectively, indicate mixed character for both, with larger Rydberg contribution for the former. Since Rydberg bands are, due to their large spatial extent, expected to be blue-shifted in condensed phase, comparison of the condensed phase and gas-phase spectra should provide evidence for the Rydberg/valence character. The peak of the first photoabsorption band of argon matrix isolated HMDS has been observed at 6.63 eV,[6] about 0.3 eV higher than in the present gas-phase spectrum. This shift appears too small for a pure Rydberg state but may well be compatible with our valence−Rydberg mixed assignment. The extent of Rydberg−valence mixing will change when going to condensed phase, the Rydberg components being shifted to higher energies, so that the lower state may be less Rydberg-like in condensed phase than in the gas phase.

The next comment concerns the $\pi^*-\sigma^*$ ordering. It has been deduced experimentally, from the polarization in stretched films,[2] that the lowest absorption band is σ^*(Si−Si) in higher linear permethylated silane oligomers and polymers. It has, however, been recognized[2] that the σ^*(Si−Si) is stabilized faster with increasing chain length and that the π^* state may well be the lowest valence state in HMDS, that is, our assignment does not contradict the earlier work. Furthermore, the $\pi^*-\sigma^*$ ordering in HMDS will depend on the Si−Si bond length, since the σ^* state is rapidly stabilized and the π^* state destabilized when the Si−Si distance increases (Figure 3). (Our preliminary calculation with R_{Si-Si} = 2.68 Å showed the HOMO → π^* vertical excitation energy nearly unchanged at 6.90 eV but the HOMO → σ^* transition greatly lowered, from 8.44 to 6.91 eV.) Thus the HOMO → σ^* state may well be the lowest adiabatic excited state even in HMDS, as proposed by Plitt et al.,[6] in particular in the condensed phase where the different degree of valence−Rydberg mixing may further affect the ordering.

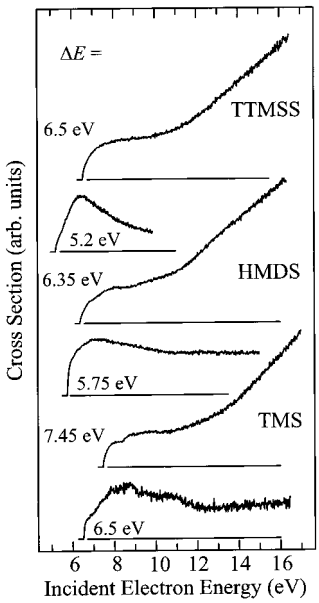

Figure 7. Excitation functions of selected electronically excited states of TMS (lower pair of curves), HMDS (center pair of curves), and TTMSS (upper pair of curves).

TTMSS has been included in the present study to evaluate the changes encountered when going from the small oligomers to (branched) polymers. An important consequence of the increasing number of Si atoms is found to be a dramatically increasing density of states: 60 singlet roots were obtained within an energy range of only 2 eV! (The calculated low-lying states are shown in Figure 4, and only few selected singlet states are listed in Table 7.) The second finding is that it becomes increasingly difficult (and arbitrary) to classify the excited states as valence or Rydberg; all wave functions are of relatively large spatial extent. This means that the nature of the states may substantially change in the condensed phase, where the diffuse components of the wave functions are perturbed by the matrix or solvent molecules.

As mentioned above, TMOS has 8 high-lying occupied MO's, all oxygen lone pairs (with some contributions from the π_{CH_3}), with calculated orbital energies between −7.16 and −8.67 eV. They give rise to a large number of Rydberg states, listed in Table 8 and indicated in Figure 5. The lowest valence singlet is HOMO → σ^* at 8.75 eV. The corresponding valence triplet (mixed with $4p_{xy}$ Rydberg) is calculated at 8.36 eV. The small singlet−triplet separation is a consequence of the small value of the lone pair−σ^* exchange integral.

3.3. Excitation Functions. Relative cross sections for electronic excitation, recorded as a function of the incident electron energy, are shown in Figure 7. The lower curve for each compound has been recorded at an energy loss ΔE just below the first singlet state. The observed shapes of these excitation functions for all three compounds are characteristic of triplet excitation: the curves peak close to threshold and then decrease continuously with increasing electron energy. The upper curve for each compound has been recorded at an energy loss where both triplet and singlet states overlap. This is reflected in the shapes; they are steplike near threshold, due to triplet excitation, and rise nearly linearly at higher energy, behavior characteristic of dipole-allowed singlet−singlet transitions.

We recorded the excitation functions of TMOS but do not show them here. They are consistent with our assignment of the EEL spectra. An excitation function recorded at an energy

loss of 7.0 eV, that is just below the steep rise in the singlet spectrum, is characteristic of a spin- and/or dipole forbidden transition: it rises steeply at threshold, has a broad maximum around 9 eV and then remains nearly flat up to 17 eV. An excitation function recorded at an energy loss of 8.4 eV, at the peak of the singlet spectrum, is characteristic of overlapping triplet and dipole-allowed singlet transitions, having a steplike rise at threshold (due to the triplet), followed by a nearly linear rise due to dipole allowed singlet excitation.

The detailed shape of a triplet excitation function differs from molecule to molecule. A remarkable feature of the triplet-state excitation functions of the present silanes is their steplike onset and consequently the relatively large value of the cross section already at and immediately above threshold. This is in contrast to the cross sections found for example in ethene[35] or benzene,[12] where the onset of the triplet cross section is more gradual and the cross section is small in the immediate vicinity of the threshold.

Electronic excitation near threshold is important in discharges, where the energy distribution of the free electrons peaks at around 1 eV and then decreases rapidly. The substantial size of the threshold cross sections for triplet excitation, in contrast to small threshold cross sections for singlet excitation, will thus cause the yield of triplet states to be much larger than the yield of the singlet states. This means that triplet states may be far more important in the chemistry of plasmas than singlet excited states.

4. Conclusions

The DFT/SCI theory is found to reproduce very well both the singlet and the triplet spectra, indicating that it is a suitable tool for describing excited states of the silanes and is potentially capable of describing their excited-state chemistry, relevant for plasma processes.

Low-lying triplet and singlet excited states of TMS are Rydberg states; the lowest valence states are found at substantially higher energy.

HMDS reveals the spectroscopic consequences of a Si−Si bond, in particular lowering of valence states relative to the Rydberg states. The lowest excited state in the triplet manifold is of valence character in this compound. The lowest singlet state is the HOMO → 4s Rydberg state, but the next higher state, a HOMO → 4p, has a substantial valence character. The upper orbital of the lowest valence transitions has a π symmetry and is, in contrast to the π^* MO of ethene, bonding across the Si−Si bond (and antibonding with respect to the Si−C distance). The HOMO → σ^* transition, with σ^* strongly antibonding across the Si−Si bond, is found higher in energy but, as a consequence of the opposite bonding/antibonding character of the upper valence MOs, becomes the lowest excited state when the Si−Si distance is stretched.

The results on TTMSS, which may be considered as a step toward branched silane polymers, emphasize the rapidly increasing density of states with increasing number of Si atoms and an increasing degree of valence−Rydberg mixing, which makes classification of the excited states as valence or Rydberg difficult and arbitrary. The nature of the excited states is consequently expected to differ significantly between the gas and condensed phases.

Strong structure−spectra relationship is born out by TMOS. Its spectra differ from those of the other silanes already in their qualitative appearance, particularly by the absence of pronounced structure. The DFT/SCI calculations rationalize this difference: the strong Si−O bond causes the $\sigma \rightarrow \sigma^*$ transitions, which would make the spectrum more structured, to be much higher in energy. There remain many lone pair → Rydberg transitions, which naturally have very similar energies. The deceivingly simple broad band at 8.4 eV in the singlet spectrum is found to be a result of about a dozen transitions.

Acknowledgment. We wish to express our sincere appreciation to Professor E. Haselbach for his continuing support and encouragement in the present work. This work is part of Project 2028-047212.96/1 of the Swiss National Science Foundation. The services and computer time made available by the Sonderforschungsbereich 334 ("Wechselwirkungen in Molekülen") have been essential to this study which was financially supported by the Deutsche Forschungsgemeinschaft.

References and Notes

(1) Lelogeais, M.; Ducarroir, M. *Thin Solid Films* **1991**, *197*, 257.
(2) Miller, R. D.; Michl, J. *Chem. Rev.* **1989**, *89*, 1359.
(3) Robin, M. B. *Higher Excited States of Polyatomic Molecules*; Academic Press: New York, 1974; Vol. I.
(4) Robin, M. B. *Higher Excited States of Polyatomic Molecules*; Academic Press: New York, 1985; Vol. III.
(5) Awazu, K.; Onuki, H.; Ibuki, T. *Jpn. J. Appl. Phys.* **1993**, *32*, L869.
(6) Plitt, H. S.; Balaji, V.; Michl, J. *Chem. Phys. Lett.* **1993**, *213*, 158.
(7) Sodhi, R. N. S.; Daviel, S.; Brion, C. E. *J. Electron Spectrosc. Relat. Phenom.* **1985**, *35*, 45.
(8) Bock, H. *Angew. Chem.* **1989**, *101*, 1659.
(9) Modelli, A.; Jones, D.; Favaretto L.; Distefano, G. *Organometallics* **1996**, *15*, 380.
(10) Winkler, D. C.; Moore, J. H.; Tossell, J. A. *Chem. Phys. Lett.* **1994**, *222*, 1.
(11) Urquhart, S. G.; Xiong, J. Z.; Wen, A. T.; Sham, T. K.; Baines, K. M.; de Souza, G. G. B.; Hitchcock, A. P. *Chem. Phys.* **1994**, *189*, 757.
(12) Allan, M. *J. Electron Spectrosc. Relat. Phenom.* **1989**, *48*, 219.
(13) Allan, M. *Helv. Chim. Acta* **1982**, *65*, 2008.
(14) Asmis K. R.; Allan, M. *J. Phys. B* **1997**, *30*, 1961.
(15) Grimme, S. *Chem. Phys. Lett.* **1996**, *259*, 128.
(16) Grimme, S. Habilitation Thesis, Bonn 1997.
(17) Bulliard, C.; Allan, M.; Smith, J. M.; Hrovat, D. A. Borden W. T.; Grimme S. *Chem. Phys.* **1997**, in press.
(18) Ahlrichs, R.; Bär, M.; Häser, M.; Horn, H.; Kölmel, *Chem. Phys. Lett.* **1989**, *162*, 165.
(19) Treutler, O.; Ahlrichs, R. *J. Chem. Phys.* **1995**, *102*, 346.
(20) Schäfer, A.; Horn, H.; Ahlrichs, R. *J. Chem. Phys.* **1992**, *97*, 2571.
(21) Callomon, J. H.; Hirota, E.; Kuchitsu, K.; Lafferty, W. J.; Maki, A. G.; Pote, C. S. *Structure Data on Free Polyatomic Molecules*; Landolt-Bronstein, New Series, Group II, Vol. 7; Springer: Berlin 1976.
(22) Becke, A. D. *J. Chem. Phys.* **1993**, *98*, 5648.
(23) Stephens, P. J.; Devlin, F. J.; Chabalowski, C. F.; Frisch, M. J. *J. Phys. Chem.* **1994**, *98*, 11623.
(24) Dunning, T.-H., Jr.; Hay, P.-J. In *Methods of Electronic Structure Theory*; Schaefer, H. F., III, Ed.; Plenum Press: New York, 1977.
(25) Bauschlicher, C. W., Jr.; Langhoff, S. R. *Theor. Chim. Acta* **1991**, *79*, 93.
(26) Schulz, G. J. *Rev. Mod. Phys.* **1973**, *45*, 423.
(27) Lee, T. J.; Bauschlicher, C. W.; Jayatilaka, D. *Theor. Chem. Acc.* **1997**, *97*, 185.
(28) Harada, Y.; Murell, J. N.; Sheena, H. H. *Chem. Phys. Lett.* **1968**, *1*, 595.
(29) Krieger, J. B.; Li, Y.; Iafrate, G. J. *Phys. Rev. A* **1992**, *45*, 101.
(30) Cole L. A.; Perdew J. P. *Phys. Rev. A* **1982**, *25*, 1265.
(31) Grimme S.; Waletzke M. Unpublished results.
(32) Pitt, C. G.; Bursey, M. M.; Rogerson, P. F. *J. Am. Chem. Soc.* **1970**, *92*, 519.
(33) Allan, M. *J. Am. Chem. Soc.* **1993**, *115*, 6418.
(34) Allan, M.; Andric, L. *J. Chem. Phys.* **1996**, *105*, 3559.
(35) Asmis, K. R.; Allan, M. *J. Chem. Phys.* **1997**, *106*, 7044.